DOI 10.48612/fpg/rada-dxbz-35be

УДК 551.46.06 + 528.8.04

© *A. V. Frolova*[1,2], *D. V. Pozdnyakov*[1,2*], *E. A. Morozov*[3], 2023

[1]St. Petersburg State University, 7–9 Universitetskaya Emb., St. Petersburg, 199034, Russia
[2]Nansen International Environmental and Remote Sensing Centre, 14th Line 7, Vasilievsky Island, St. Petersburg, 199034, Russia
[3]Marine Hydrophysical Institute, Kapitanskaya Str., 2, Sevastopol, 299011, Russia
*d.pozdnyakov@spbu.ru; dmitry.pozdnyakov@niersc.spb.ru

A SATELLITE STUDY OF THE *E. HUXLEYI* PHENOMENON IN THE BARENTS, NORWEGIAN, AND GREENLAND SEAS IN 2003–2021: TEMPORAL DYNAMICS OF THE BLOOM AREAL EXTENT, INORGANIC CARBON PRODUCTION AND CO_2 PARTIAL PRESSURE IN SURFACE WATER

Received 04.07.2022, Revised 22.11.2022, Accepted 15.01.2023

Abstract

Based on satellite data, *E. huxleyi* bloom contouring, quantification of particulate inorganic carbon (PIC) production and increment of CO_2 partial pressure, (pCO_2) in surface water were performed. 18-year (2003–2021) time series of these variables are obtained for the Norwegian, Greenland and Barents seas. The bloom areas in the North Atlantic–Arctic water are the lowest in the Greenland Sea varying from 10×10^3 km^2 to $(20–40)\times10^3$ km^2. In the Norwegian and Barents Seas they reach in some years $(60–80)\times10^3$ km^2 and $(500–600)\times10^3$ km^2, respectively. The total PIC content within *E. huxleyi* blooms rarely exceeds in the Greenland and Norwegian seas 12–14 kilotons and 40 kilotons, respectively. In the Barents Sea, in some years, it can be up to 550 kilotons. The highest level of pCO_2 within *E. huxleyi* blooms in surface waters in the Barents Sea was ~350 μatm. In the Norwegian Sea, pCO_2 in surface waters within the *E. huxleyi* bloom was also close to 350 μatm, but most often it remained about 250 μatm. In the Greenland Sea there were only four years of relatively enhanced pCO_2 (up to 250 μatm), otherwise remaining below the level of confident determination by our method. As *E. huxleyi* blooms are generally very extensive, occur throughout the entire World Oceans (and hence in sum occur all year around), this phenomenon has a potential to both decrease to some degree the role of the World Oceans as sinkers of atmospheric CO_2, and affect the carbonate counter pump.

Keywords: Satellite remote sensing of *E. huxleyi* blooms, 18-year time series of bloom surface, production of inorganic carbon, bloom-driven increase in CO_2 partial pressure, effect of preseeding, the Gulf Stream, influence on ocean-atmosphere CO_2 fluxes and carbonate counter pump

© *А. В. Фролова*[1,2], *Д. В. Поздняков*[1,2*], *Е. А. Морозов*[3], 2023

[1]Санкт-Петербургский государственный университет, 199034, Университетская наб., 7–9, Санкт-Петербург, Россия
[2]Научный Фонд «Международный центр по окружающей среде и дистанционному зондированию имени Нансена», 199034, 14-я линия Васильевского острова, 7, Санкт-Петербург, Россия
[3]Морской гидрофизический институт, 299011, Капитанская ул., 2, Севастополь, Россия
*d.pozdnyakov@spbu.ru; dmitry.pozdnyakov@niersc.spb.ru

СПУТНИКОВОЕ ИССЛЕДОВАНИЕ ФЕНОМЕНА ЦВЕТЕНИЙ *E. HUXLEYI* В БАРЕНЦЕВОМ, НОРВЕЖСКОМ И ГРЕНЛАНДСКОМ МОРЯХ В 2003–2021 ГГ.: ВРЕМЕННАЯ ДИНАМИКА АРЕАЛА ЦВЕТЕНИЙ, ПРОДУКЦИИ НЕОРГАНИЧЕСКОГО УГЛЕРОДА И ПАРЦИАЛЬНОГО ДАВЛЕНИЯ CO_2 В ПОВЕРХНОСТНЫХ ВОДАХ

Статья поступила в редакцию 04.07.2022, после доработки 22.11.2022, принята в печать 15.01.2023

Аннотация

На основе спутниковых данных проведен анализ цветения *E. huxleyi*: количественная оценка продукции взвешенного неорганического углерода (PIC) и увеличения парциального давления CO_2, (pCO_2) в поверхностных водах. Временные ряды этих переменных были получены для Норвежского, Гренландского и Баренцева морей за 18-летний

Ссылка для цитирования:*Фролова А.В.*, *Поздняков Д.В.*, *Морозов Е.А.* Спутниковое исследование феномена цветений *E. huxleyi* в Баренцевом, Норвежском и Гренландском морях в 2003–2021 гг.: временная динамика ареала цветений, продукции неорганического углерода и парциального давления CO_2 в поверхностных водах // Фундаментальная и прикладная гидрофизика. 2023. Т. 16, № 1. С. 48–62. doi:10.48612/fpg/rada-dxbz-35be

For citation: *Frolova A.V.*, *Pozdnyakov D.V.*, *Morozov E.A.* A Satellite Study of the *E. huxleyi* Phenomenon in the Barents, Norwegian, and Greenland Seas in 2003–2021: Temporal Dynamics of the Bloom Areal Extent, Inorganic Carbon Production and CO_2 Partial Pressure in Surface Water. *Fundamental and Applied Hydrophysics*. 2023, 16, 1, 48–62. doi:10.48612/fpg/rada-dxbz-35be

период (2003–2021 гг.). Площади цветения в североатлантических и арктических водах наименьшие в Гренландском море — от 10×10^3 км^2 до $(20–40)\times10^3$ км^2. В Норвежском и Баренцевом морях они достигают в некоторые годы $(60–80)\times10^3$ км^2 и $(500–600)\times10^3$ км^2, соответственно. Общее содержание PIC в цветении *E. huxleyi* редко превышает 12–14 килотонн и 40 килотонн в Гренландском и Норвежском морях, соответственно. В Баренцевом море в некоторые годы оно может достигать 550 килотонн. Наибольшее значение pCO_2 во время цветения *E. huxleyi* в поверхностных водах Баренцева моря составило ~350 мкатм. В Норвежском море pCO_2 в поверхностных водах в пределах цветения *E. huxleyi* также было близко к 350 мкатм, но чаще оставалось около 250 мкатм. В Гренландском море было только четыре года относительно повышенного pCO_2 (до 250 мкатм), в остальное время он оставался ниже уровня уверенного определения нашим методом. Поскольку цветения *E. huxleyi* обычно очень обширны, происходят по всему Мировому океану (и, следовательно, в совокупности происходят круглый год), это явление потенциально может как снизить до некоторой степени роль Мирового океана как поглотителя атмосферного CO_2, так и повлиять на карбонатный насос.

Ключевые слова: Спутниковое дистанционное зондирование цветения *E. huxleyi*, 18-летний временной ряд площади цветения, производство неорганического углерода, вызванное цветением увеличение парциального давления CO_2, эффект предварительного засева, Гольфстрим, влияние на потоки CO_2 из океана в атмосферу и карбонатный насос

1. Introduction

The anthropogenically-caused increase in the content of carbon dioxide, CO_2, in the atmosphere predominantly determines the observed global warming [1]. At the same time, the efficiency of the World Ocean, the main reservoir of atmospheric CO_2 sink, gradually deteriorates as the reaction of dissolution of CO_2 gradually moves towards saturation. With the ongoing warming of the ocean surface, the dynamic equilibrium shifts between the dissociated and suspended forms of calcite, $CaCO_3$. This, in turn, causes an increase in the process of acidification of the surface waters of the ocean [2, 3], which in turn triggers the process of transformation of the biotic system in the ocean along the chain of biogeochemical reactions [4].

In the marine phytoplankton community, coccolithophores are the main calcifiers, i. e. producers of suspended $CaCO_3$. In this group of microalgae in pelagic waters, the most widespread and effective $CaCO_3$ producer is *Emiliania huxleyi* [5].

Moreover, some of the CO_2 molecules released in the calcification reaction [6] are used by *E. huxleyi* cell for photosynthesis, thus decreasing the need of the cell in CO_2 dissolved in water and enhancing the partial pressure, pCO_2, in surface water within the bloom area. As a result, the atmospheric CO_2 flux into the blooming area should decrease. Thus, the ability of *E. huxleyi* to produce particulate inorganic carbon (PIC), and enhance pCO_2 lends this microalga a significant role as a climatological factor. For this reason, the study of occurrence of *E. huxleyi* blooms, their spatial extent and intensity in the waters of the World Ocean is of importance.

As a rule, the spatial extent (S) of *E. huxleyi* blooms and their temporal variability [7] are generally very significant, and this necessitates the use of remote sensing observations along with shipboard studies.

The start to remote observations of *E. huxleyi* blooms was prompted by the pioneering work of Holligan et al. [8]. Further on, satellite-based studies were continued and developed in a number of studies.

Based on the application of spaceborne ocean colour data, many of remote sensing observations of *E. huxleyi* were focused on identification of blooms of these algae in some limited locations of World Ocean [9–17]. Somewhat fewer publications were reported on quantifications of both bloom extent and the concentration of PIC [17–19]. Some articles were focused on establishing the time series of quantified parameters characterizing coccolithophore blooms [11, 14, 16, 17, 20–23]. The length of the published time series of data on coccolithophore blooms varies significantly, and possibly the longest one (1997–2011) is that reported by [17] for the bloom areas and cumulative/summated PIC values across the World Oceans. In a latter publication, [7] reported on a 16-year (1998–2013) series of bloom areal extent, *S*, and PIC production by *E. huxleyi*, but solely in subpolar and polar seas.

It was found that ocean colour remote sensing data could also be used to retrieve *E. huxleyi*-driven pCO_2 increment, ΔpCO_2 [24]. The impact of *E. huxleyi* bloom on CO_2 fluxes between the atmosphere and ocean was confirmed in a series of spaceborne case studies performed by Morozov et al. [25] in some North Atlantic and Arctic seas.

In the present paper, based on the methodologies developed by Kondrik et al. [7, 24], we investigate the spatio-temporal variations in *S*, ΔpCO_2, and PIC within the blooms of *E. huxleyi* in the Norwegian, Greenland and Barents seas over the time period 2003–2021. This selection of seas is dictated by the previous findings (dating back to 1998–2013) that the *E. huxleyi* blooms are most extensive and intense as compared to other areas in the North Atlantic and Arctic [26]. That is why it was of interest to expand the time interval of observations, bringing it closer to the present time in order to examine the contemporary features in the dynamics of the *E. huxleyi* blooming phenomenon.

2. Data sources

2.1. Ocean colour data

To investigate multi-year dynamics of ocean colour features of marine environments, harmonized bridging/merging of multi-sensor spaceborne data at the desired spatial and temporal resolution are mandatory. The GlobColour product [27] was employed in this study. In the early 2018, the processor has been modified to apply a lower level of flagging, resulting in a better spatial and temporal coverage. According to the GlobColor User Guide, in 2020 all NASA sensors readings, including new error bars, were updated to R2018.0 in the entire archive. Data spatial and temporal resolution is 4 by 4 km and 8 days, respectively.

The data used in this study were developed, validated, and distributed by ACRI-ST (European Marine Observation and Data Network), France. In our case, images in 6 channels (412, 443, 490, 531, 555, 670 nm) were employed. Although data on spectral remote sensing reflection, $R_{rs}(\lambda)$, also can also be found in other data sources (e.g. OC–CCI (Ocean Color Climate Change Initiative), MEaSUREs (Making Earth Science Data Records to use in research environments)), however, the consistency of the long time series provided by them suffers more from some limitations due to problems with sensors [28].

Data resolution and projection. In our analyses, one month and 4 km by 4 km data resolution was used. Given the latitudinal location of the seas addressed in this study, the EPSG:4326 projection (the WGS84 (World Geodetic System 1984) Coordinate Systems whose unique reference code, the so-called EPSG code which is 4326) was applied [29].

2.2. Sea surface temperature (SST) data

To obtain SST, we applied the NOAA satellite dataset [30] at a 4 km by 4 km spatial and twice-daily (night) resolution from the Pathfinder v5.3 level 3 collated (L3C) product based on the Advance Very High Resolution Radiometer (AVHRR) measurements over the 1981-present period [31,32].

2.3. Sea surface salinity (SSS) and nitrates, NO_3^- data

SSS and nitrates data at 1° by 1° spatial and daily resolution for the time period 1955–2017 are from the World Ocean Atlas 2018 (WOA18) [33].

The WOA18 in situ data (more than 15.7 million oceanographic casts made up of 3.56 billion individual profile measurements), were collected in the World Ocean Database, interpolated over the 1° by 1° and averaged over time period 1955–2017.

To harmonize the time resolution of the input data, the temporal resolution for SSS, SST, NO_3 were brought to that of the GlobColour, that is 8 days.

3. Methodology

3.1 Radiometric parameter and bloom area quantification

Defined as the above water surface upwelling spectral radiance normalized to the atmospherically corrected spectral irradiance, the spectral remote sensing reflection, R_{rs} (λ), is one of the fundamentally important parameters provided by a number of satellite products of different processing levels. Being a convolution of light interactions with all co-occurring water constituents, $R_{rs}(\lambda)$ is instrumental in solving inverse problems of marine remote sensing including the retrieval of the parameters which are the subject of the present study.

The statistical data analysis of the $R_{rs}(\lambda)$ spectral curvature associated with *E. huxleyi* blooms revealed that the R_{rs} maximum can locate at either 510 nm or 490 nm depending upon the phase of the bloom development: the first location is inherent in the earlier stages of bloom formation and is due to a joint effect of backscattering of coccoliths and pigment absorption, while the second location is indicative of a senile bloom that is populated mostly by coccoliths and mainly died algal cells. These features permitted to accurately delineate *E. huxleyi* blooms but also draw conclusions on their life cycle stage. Additional thresholds for R_{rs} spectral values (sr^{-1}) [>0.001, >0.008, >0.01, > 0.005, 0.005–0.05, ~0 at respectively 412, 443, 490, 531, 555 and 670 nm] deduced from the aforementioned statistical data analysis helped improve the efficiency of *E. huxleyi* contouring [7].

3.2. Cloud masking problem mitigation

To mitigate the problem of cloud-masking and associated loss of data, the following averaging procedure was applied: $R_{rs}(\lambda)$ values from pixels adjacent to the cloud-masked one were averaged together with the $R_{rs}(\lambda)$ values from the cloud-masked pixel but taken from the immediately preceding and following 8-day periods. The efficiency of this approach was evaluated in [7].

3.3. Quantification of particulate inorganic matter PIM; the BOREALI algorithm

Quantification of the concentration of particulate inorganic matter in the form of coccoliths (PIM), was performed with the BOREALI (Bio-optical Retrieval Algorithm) algorithm [26] which is a multivariate optimization procedure permitting, in our case, to restore from $R_{rs}(\lambda)$ the concentration vector of co-occurring colour producing agents, CPAs. As CPAs, we considered water per se, phytoplankton, coined here as Chl-a, PIM (in the case of *E. huxleyi* blooms, PIM ≡ coccoliths), and coloured dissolved organic matter, CDOM. Running of the BOREALI algorithm requires a hydro-optical model of the waters prone to remote sensing, i.e. spectral specific absorption and backscattering coefficients of each CPA. The inverse problem solution is based on the iterative procedure of assessing the function f(C) of squares of residuals of the difference between the observed/retrieved and simulated values of R_{rsw}, which is the subsurface remote sensing reflectance defined as the upwelling spectral radiance just beneath the water–air interface normalized to the downwelling spectral irradiance at the same level [34]. Thus, R_{rsw} and R_{rs} are both the spectral remote sensing reflectance, but R_{rs} defined as the ratio of upwelling radiance just above the air-water interface and the downwelling irradiance at the same level.

As there are parameterizations (equation of their liner dependence) relating R_{rsw} and R_{rs} [35], $R_{rsw}(\lambda)$ can be obtained from the GlobColour product we used.

Through varying the concentration vector $\mathbf{C} = [1, \text{Chl-}a, \text{PIM, CDOM}]$ (1 stands for water per se), and minimization at each wavelength of the function $f(\mathbf{C})$, the absolute minimum can be found, e.g. with the Levenberg–Marquardt finite difference algorithm [36]. The value of **C** obtained on attaining the absolute minimum of the function $f(\mathbf{C})$ is the solution of the inverse problem. Thus, this technique permits retrieving simultaneously all CPA components of the concentration vector **C**. Simulated spectral values of R_{rsw} were obtained via employing the parameterization suggested by Jerome, et al. [34].

The hydro-optical model employed in this study is taken from Kondrik et al. [7]. This model was thoroughly validated and showed the following statistical characteristics: correlation coefficient, $R = 0.88$; linear regression equation, $f(x) = 0.6159x + 6.9197$; determination coefficient, $R^2 = 0.77$; root mean square error, $RMSE = 3.55 \times 10^9$ coccoliths m^{-3}; systematic error, $BIAS = 25.30\,\%$; mean absolute error, $MAE = 32.30\,\%$.

In addition to PIM (particulate inorganic matter, i.e. the coccoliths) quantification, the results of the BOREALI algorithm application were also used to define more precisely *E. huxleyi* bloom areas via applying a threshold of 90×10^9 coccoliths $\times m^{-3}$. The latter assures the closest correspondence between the bloom surfaces assessed by our radiometric and BOREALI algorithms. Besides, it agrees well with the average coccolith concentrations in developed *E. huxleyi* blooms reported from the World Ocean [10, 37].

3.4. Determination of inorganic particulate carbon (PIC)

The total content of PIC was determined for each 8 day-time period through multiplication of the carbon mass per coccolith, *m*, i.e. PIM, mixed layer depth, MLD, and the bloom area, *S*. The PIC assessment of over the entire bloom area was performed through averaging PIC values in each pixel. The value of *m* was equaled to 0.2 pg [37,7]. The moment, at which the PIC assessment could be ideally performed in each bloom, corresponded to the situation when two conditions were fulfilled: (*a*) the bloom attained its largest surface and (*b*) the spectral curvature of remote-sensing reflectance, $R_{rs}(\lambda)$, exhibited a maximum at about 490 nm (bearing in mind that the location of the maximum at about 490 nm indicates that the bloom is prevalently composed of coccoliths, see Section 3.1). The relevance of choosing the stage when the bloom area is largest as the moment of determining PIC content might be underpinned by the following considerations. Given that during the vegetation period, the typical MLD extent in the target seas rarely exceeds 20 m [38] and the coccolith sinking rate assessed in the literature is about $0.1\ m \times day^{-1}$ [39]; the coccolith concentration determined at the conditions specified above must be truly representative. However, in real-life conditions, the composition of *E. huxleyi* blooms is at any time heterogenous encompassing the areas with $R_{rs}(\lambda)$ peaking at 490 and 510 nm. That is why the BOREALI algorithm was applied within the entire bloom to 8 day-averaged images permitting to overcome the above impediment and obtain the desired time series.

3.5. Determination of the mixed layer depth (MLD) within E. huxleyi blooms

To retrieve the columnar values of PIM and then PIC, the value of MLD needed to be available across the target bloom area. In situ determinations of SST and SSS at individual stations are appropriate for our aims because only spatially continuous MLD are required. This is why we addressed the climatological data provided Montegut et al. [38]. The reasoning of this selection is given in more detail in Kondrik et al. [7].

3.6. Determination of ΔpCO_2

The previously established relationship between ΔpCO_2 and R_{rs} at $\lambda = 490$ nm [$\Delta pCO_2 = 3926.466 \times R_{rs}(490) + 3.22$; $R^2 = 0.54$, probability that the null hypothesis correct, $p \ll 0.001$, and RMSE = 23.4 μatm; total number of in situ data = 2615 collectively from GLODAP and WOA13] [7] was used to quantify the bloom-driven increments ΔpCO_2. Values of ΔpCO_2 were firstly corrected for the standard temperature (10 °C) and then corrected for the respective background values of pCO_2, $(pCO_2)_b$, to yield the desired bloom-driven increments ΔpCO_2 under the standard conditions. The above equation was further applied to all detected *E. huxleyi* blooms to retrieve ΔpCO_2 values in each pixel, firstly, at 10 °C. This was then followed by bringing the determined ΔpCO_2 values to the actual SST and SSS through employing equations (S2)–(S8) given in Kondrik et al. (Appendix) [24]. The background partial pressure of CO_2, $(pCO_2)_b$ was numerically assessed at a "standard" temperature 10 °C through making use of the climatological database of the concentration of nitrates NO_3^- dissolved in waters adjacent to *E. huxleyi* bloom areas (See Kondrik et al. [24] for details).

4. Results and discussion

4.1. Temporal dynamics of bloom areas, S, and particulate inorganic carbon, PIC, production

Fig. 1 illustrates the identified *E. huxleyi blooms* as well as their surficial extent and associated PIC values production in the seas addressed in this study for the time period 2003–2021.

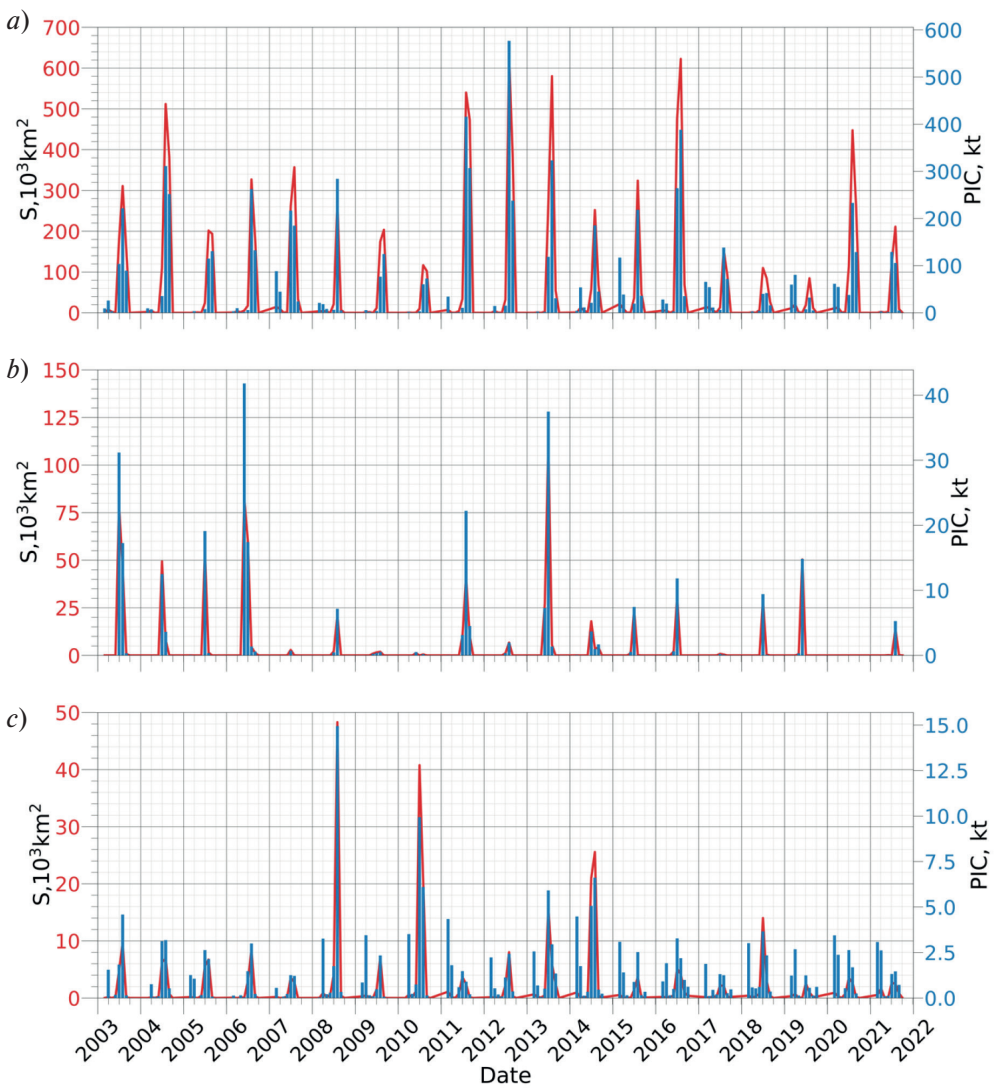

Fig. 1. Interannual dynamics of *E. huxleyi* outbursts, respective bloom surfaces (defined with our spectral algorithm) and within-bloom inorganic carbon contents (designated in blue and red, respectively) as retrieved from space across the target seas over 2003–2021: (*a*) Barents Sea, (*b*) Norwegian Sea, and (*c*) Greenland Sea

4.1.1. Barents Sea

Our space-based observations are indicative that *E. huxleyi* blooms in the Barents Sea occur annually, although their intensity is subject to significant variations. In some years (specifically, in 2004, 2011, 2012, 2013, 2016, 2020), blooms occupied very large areas mounting up to (500–600)×10^3 km^2. However, such occasions alternate with the years of remarkably subdued activity of *E. huxleyi* bloom development, especially during 2017–2019. A somewhat reduced blooming activity also fell on 2009 and 2010. However, even in the years of relatively low bloom development, the bloom areas were about 100×10^3 km^2, which is remarkable in itself. The highest levels of PIC production were in excess of (400–550) kt, but even low levels were, nevertheless, at about (50–150) kt.

It is noteworthy that the values of peak bloom areas do not necessary correspond with the peak values of PIC production and vice versa, which has a natural explanation: large bloom areas are not necessary densely populated with coccoliths, and contrarily, even small-size blooms can be relatively efficient in producing PIC.

As Fig. 1 illustrates, there is no clear trend in interannual variations of either *E. huxleyi* bloom surface or PIC production, although some sort of an indication of a quasi-sinusoidal pattern of the conjoint variation in both parameters can be tentatively supposed.

4.1.2. Norwegian Sea

Similar to the Barents Sea, the pattern of *E. huxleyi* outbursts was expressly irregular: relatively large blooms with an area within (40–80)×10^3km^{2}alternated with rather long periods of relatively low population growth intensity of this microalgae. The strongest outburst occurred in 2013, and since then the bloom areas did not exceed some (20–40)×10^3km^2.

It is possible to suppose that the blooms in this sea are characterized by dense populations of coccoliths because in all bloom cases the PIC production was appreciably high, in some years exceeding (30–40) kt in the blooms of a rather moderate surficial extent as compared with e.g. the Barents Sea.

The time series illustrated in Fig. 1 for this sea leaves an impression that since 2013 there is a trend of a gradual decline in the intensity of *E. huxleyi* growth in this sea. This impression is reinforced by the declining tendency (over the time period 1998–2013) in S previously revealed in Kondrik et al. [7].

4.1.3. Greenland Sea

As compared to the Norwegian Sea and especially the Barents Sea, the Greenland Sea is characterized by a far less significant intensity of *E. huxleyi* growth and formation of blooms. Over the entire period 2003–2021, there were only three relatively extensive bloom events in 2008, 2010, and 2014, although all of them were of about (20–40)×10^3 km^2. At the same time, small-scale blooms (<10×10^3 km^2) occurred annually. The PIC production was also at low levels: in the majority of bloom events, it remained at about 3–4 kt, with the exception of 2008, 2010, 2013, and 2014 when it reached ca. 15 kt, 10 kt, and 6 kt, respectively.

4.2. Temporal dynamics of pCO_2 and ΔpCO_2 within E. huxleyi blooms through 2003–2021

Fig. 2 illustrates for the time period 2003–2021 the quantified interannual variations of marine surface water enrichment with CO_2 partial pressure within *E. huxleyi* blooms in the seas addressed in this study.

4.2.1. Barents Sea

The increase of pCO_2 in surface waters within *E. huxlyei* blooms in the Barents Sea was most significant among the seas targeted in this study. In some years (2003, 2011) the resultant, $[(pCO_2)_b + \Delta pCO_2]$, partial CO_2 pressure was as high as ~350 μatm. Many years were marked by the respective values appreciably above 300 μatm, and they practically never dropped below 250 μatm.

As Table 1 illustrates, the mean maximum increase in pCO_2 within *E. huxleyi* blooms in the Barents Sea over the time period 2003–2021 constituted 62.5%, whereas the maximum was 97.4%. Such an assessment of the above maximum mean-yearly values $[\Delta pCO_2/(pCO_2)_b]$ provides a clear vision of the CO_2 emission in the atmospheric boundary layer.

4.2.2. Norwegian Sea

The increase in pCO_2 in surface waters during the *E. huxlyei* bloom in the Norwegian Sea was the second highest after the Barents Sea. Indeed, only in one single year, 2011, the resultant, $[(pCO_2)_b + \Delta pCO_2]$, partial CO_2 was also

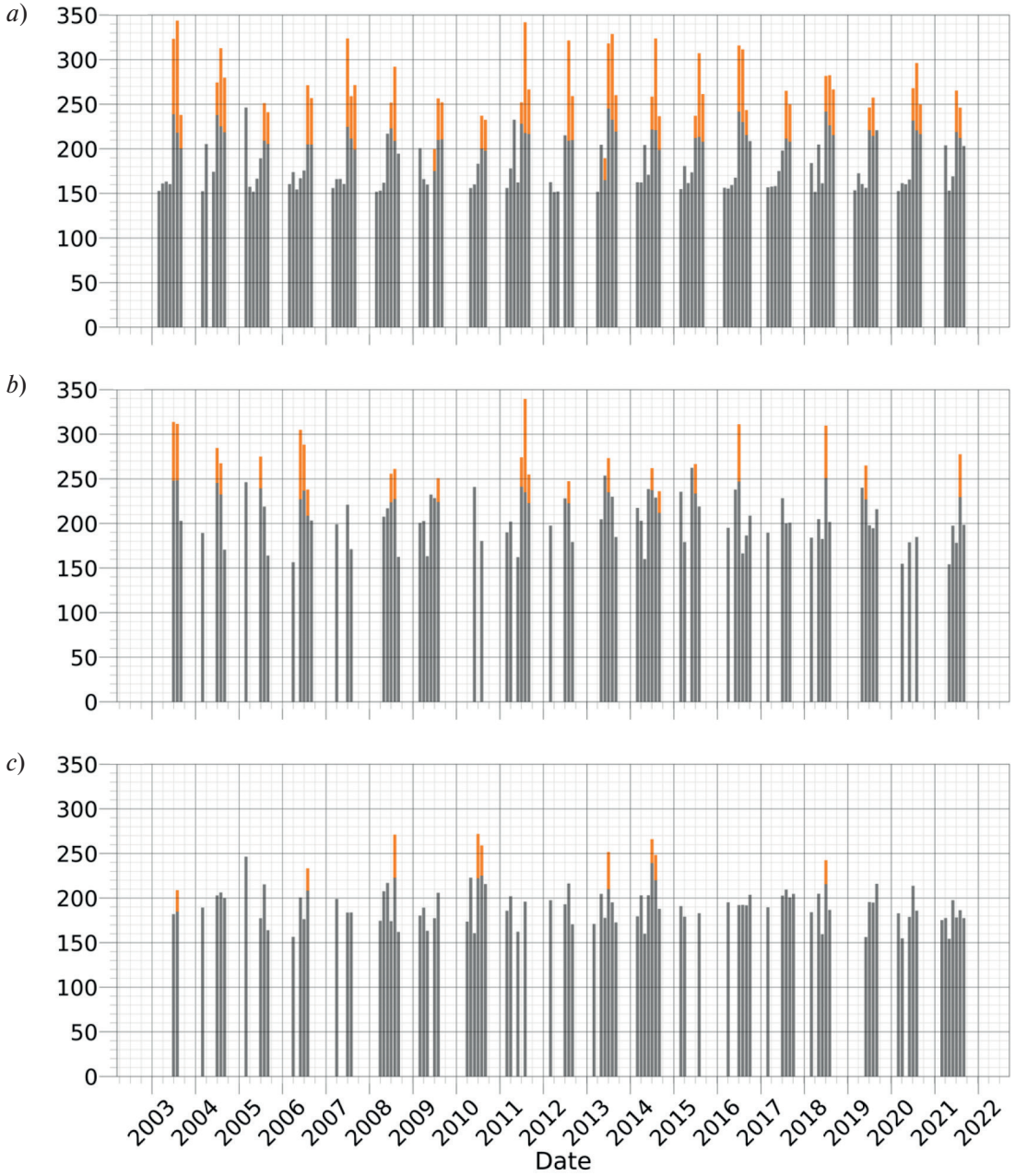

Fig. 2. Temporal variations in mean-monthly values in both $(pCO_2)_b$, μatm — gray bars, and $[(pCO_2)_b + \Delta pCO_2]$, μatm — orange bars in the Barents, Norwegian, and Greenland Seas (*a, в, c*, respectively) during 2003–2021

close to 350 μatm, and only four times (in 2003, 2006, 2016, and 2018) it exceeded 300 μatm, whereas most often it remained about 250 μatm. Remarkably, the above years of large bloom formation in the Norwegian Sea correspond, at least partially, with the years of extensive blooms in the Barents Sea.

The mean relative increment in pCO_2 driven by *E. huxleyi* blooms over the time period 2003–2021 is 46.4 %, and the maximum value of this parameter over the same time interval was 88.8 %.

4.2.3. Greenland Sea

The Greenland Sea is the least active in terms of both production of extensive *E. huxleyi* blooms (Fig. 1) and enrichment of surface waters with dissolved CO_2 (Fig. 2). There was only four years of relatively enhanced growth of this alga: in 2008, 2010, 2013, and 2014. In those years pCO_2 within the bloom area reached 250 μatm, remaining in other years below the level of confident determination by our method.

Table 1

Interannual variations in maximum mean-yearly values of the *E. huxleyi* bloom-driven increase in CO_2 partial pressure, ΔpCO_2, in surface water over the bloom area with respect to the respective background value, $(pCO_2)_b$, i.e. $[\Delta pCO_2/(pCO_2)_b]\times 100\,\%$. Notes: 1. the data are absent for some outbursts in the target seas as the respective ΔpCO_2 values proved to be lower the assessed retrieval error of 23.4 µatm [7]. 2. the mean (*) and maximal (**) values of $[\Delta pCO_2/(pCO_2)_b]\times 100\,\%$ over the time period 2003–2021 do not consider the years of near-zero values of this parameter

Year	$[\Delta pCO_2/(pCO_2)_b]$ max (%)		
	Barents Sea	Norwegian Sea	Greenland Sea
2003	81.4	88.8	20.9
2004	66.1	48.3	12.4
2005	49.2	25.4	13.4
2006	45.9	79.1	29.2
2007	77.0	32.2	
2008	40.9	36.9	69.5
2009	60.8	21.0	22.8
2010	46.1		48.2
2011	97.1	54.2	
2012	97.0	22.6	31.3
2013	76.4	37.8	33.5
2014	58.2	16.8	25.8
2015	58.1	44.4	
2016	88.4	56.5	
2017	39.7		
2018	66.4	66.8	23.7
2019	34.7	56.7	
2020	45.0		
2021	58.2	54.2	
Time period 2003–2021 mean*	**62.5**	**46.4**	**30.1**
Time period 2003–2021 max**	**97.1**	**88.8**	**69.5**

This situation found its reflection in the data illustrated in Table 1: the mean increase in pCO_2 within *E. huxleyi* blooms in the Greenland over the time period 2003–2021 did not go beyond 30.1 %, whereas the maximum did not surpass 70 %.

4.2.4. Intra-annual variations of E. huxleyi blooms

Although this is beyond the major focus of our present study, we also considered the intra-annual variations of *E. huxleyi* blooms throughout the time period of our spaceborne observations.

Figure 3 reveals that in the North and Norwegian Seas the earliest monospecific blooms of *E. huxleyi* occur in early June. Further on, they advance northward to the Greenland Sea (beginning of July), and arise in the Barents Sea by the beginning of August. On some specific years, the onsets of *E. huxleyi* blooming were found to be shifted to somewhat later dates, namely, up to mid-July in the North Sea, mid-August in the Norwegian Sea, and early September in the Barents Sea. Nevertheless, in all target seas the major blooming events occur once a year, and exclusively during the warm time period.

The intra-annual localization of the bloom within a concrete sea does not remain sedentary but can displace. Thus for instance, the blooming in the North Sea is often initially located at its northwestern boundary (in the vicinity of the northern extremity of Scotland) but further on it moves out ward forking along the British coastline and towards the southern coastal zone of Norway. Only after that the bloom starts extending over the central North Sea.

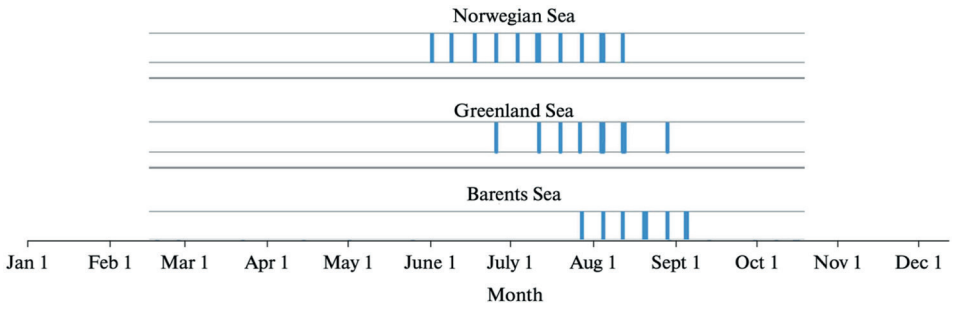

Fig. 3. Intra-annual variations of timing of *E. huxleyi* peak bloom onset in the target area

The bloom in the Norwegian Sea forms in the central and southern shore zone nearly simultaneously with the aforementioned blooming neighboring Scotland. Further on the bloom gradually displaces to the northern part of the Norwegian Sea.

The above temporal sequence is presumably dictated by the Gulf Stream specific features. Indeed, its main branch splits in the region of the north-western Scotland to further proceed to the southern coastal zone of Norway, and to the central North Sea along the coast of Scotland and England. The other (weaker) branch of the Gulf Stream (detached from the main stream at lower latitudes) moves to Greenland and rounds it.

Prior to starting the aforementioned chain-like movement from the North Sea further north to the Norwegian, Greenland and Barents Seas, the bloom emerges at the very southern extremity of the British Islands and then develops along the western and north-western coast of this Island State, rounds it and goes on the way discussed above.

Not illustrated here, our data have not revealed any definite tendency in variations regarding the duration of blooming periods. At the same time, some factors (such as the enhancement or decay of MLD) can significantly affect the blooming duration and even result in bloom suppression Pozdnyakov et al. [41]. This might be an explicit indication that the conditions for *E. huxleyi* growth were very unfavorable in those years and seas.

4.2.5. Discussion

Comparing the data presented above on variations of bloom surface *S*, PIC production as well as pCO_2 enhancement within *E. huxleyi* blooms in three target seas, several sea-specific features can be identified.

Firstly, the incidence of peak blooms in the Norwegian and Greenland seas was irregular. They arose in "batches" preceded and followed by the periods of significant decline in *E. huxleyi* population growth.

In the Norwegian Sea, peak blooms occurred in the same years as in the Barents Sea, albeit in the latter sea the years of peak blooms were much more numerous. Contrarily, in the Greenland Sea, the years of those few peak blooms recorded in our study, completely differ from those in the other seas. It might be tentatively conjected, that at least some the pick blooms in the Barents Sea were initiated through the mechanism of "preseeding" [40]. The latter implies that *E. huxleyi* living cells from intense blooms in the Norwegian Sea were transported by the Gulfstream further north, up to the Barents Sea and then triggered therein a new vast bloom. Obviously, the "preseeding" mechanism is not the only one conditioning the outbursts of *E. huxleyi* in the Barents Sea as well as in all other marine locations of this phenomenon: a favorable combinations of multiple environmental factors, such as SST, SSS, alkalinity/acidity, water column stratification, water movements (currents, eddies, fronts, advection), availability of nutrients and trace metals, viruses, microzooplankton grazing, seeding, water surface illumination, wind and wave driven surface water mixing, large-scale atmospheric baric formations and air mass transport, atmospheric CO_2 partial pressure (pCO_2), and teleconnections [41]. Clearly, the situations favoring the massive outbursts of *E. huxleyi* in the Barents Sea occur regularly/annually.

Unlike the Barents Sea, the "preseeding" mechanism as such is not enough to trigger *E. huxleyi* blooms in the Greenland Sea: the weaker branch of the Gulf Stream that reaches this sea does not bring enough cell "seeds" to start new blooms, and their origin resides in the influence of the aforementioned environmental factors.

Regarding the temporal sequence of *E. huxleyi* outbursts in the target seas, the blooms first appear in the Norwegian Sea, then in the Greenland Sea, and only after that in the Barents Sea. This is in full agreement with the findings reported earlier by Kondrik et al. [7], who have hypothesized that, concertedly with environmental forcing, the Gulf Stream conditions the propagation *E. huxleyi* blooms from the English Chanell and western coastal zone of England into the North Atlantic and Arctic.

The *E. huxleyi*-driven PIC production is expressly sea-specific: it is the highest in the Barents Sea (maximum values reached hundred thousand kilotons), whereas in the Greenland Sea, most often, it varied within several kilotons, and only on a couple of occasions it exceeded 12–14 kilotons. The Norwegian Sea occupies an intermediate position in this regard.

Data reported in Table 1 are strongly indicative that *E. huxleyi* blooms can significantly contribute to CO_2 partial pressure in surface water within the bloom area. Indeed, in the case of the Norwegian, and especially the Barents Seas, the recorded maximum increment can nearly double the respective background value. As mentioned above, this can reduce the absorptive capacity of the marine surface water with regard to atmospheric CO_2, and this was confirmed by Morozov et al. [25] for the North Atlantic: on average, the column-average content of CO_2 in the atmosphere over the *E. huxleyi* blooms showed an increase by about 1–2 ppmv. Fig. 2 and Table 1 illustrate that at least in the Norwegian Sea and especially the Barents Sea there is no distinct tendency towards a decrease of this phenomenon during the time period 2003–2021. It is also noteworthy, that our data have demonstrated that there was no direct proportion between the bloom surface and the respective increment of ΔpCO_2, as the letter is regulated by the actual density of coccoliths within the bloom.

A comparison of S, PIC and ΔpCO_2 values reported in this study with the respective data by Kondrik et al. [7] shows that the latter estimations are appreciably underestimated. Given that methodologically both studies are absolutely identical, the reason of this inconsistency should reside in the input satellite data. Indeed, we utilized the GlobColour product: in 2020 all NASA radiometric characteristics were reevaluated/updated to R2018.0 version for the entire archive (including new error bars), whereas Kondrik et al. [7] used the OC CCI database. Obviously, the refined GlobColour radiometric sensitivity proved to be higher, which permitted to obtain more accurate estimates of the desired parameters.

5. Concluding remarks

Based on the previously developed remote sensing methodologies and retrieval algorithms, 2003–2021 time series of *E. huxleyi* bloom extent, S, concentration of particulate inorganic carbon, PIC, and CO_2 partial pressure increment, ΔpCO_2, in surface water within the bloom were obtained for the Norwegian, Greenland and Barents seas.

The obtained time series for the three seas revealed no trend in the temporal dynamics of the above parameters. *E. huxleyi* bloom in the Barents Sea occurs annually, although its intensity was subject to significant fluctuations, ranging between ~ 600×10^3 km^2 and ~ 50×10^3 km^2. In the Norwegian Sea, the pattern of outbursts of *E. huxleyi* was expressly uneven: relatively large blooms with an area of ~ $(40–80)\times10^3$ km^2 alternated with fairly long periods of relatively low growth intensity of this microalgae. There were only three relatively extensive blooms in 2008, 2010 and 2014, although they all had an area of about $(20–40)\times10^3$ km^2. At the same time, small-scale blooms ($<10\times10^3$ km^2.) occurred annually.

The *E. huxleyi*-driven PIC production was expressly sea-specific: it was the highest in the Barents Sea (maximum values reached hundred kilotons), whereas in the Greenland Sea, most often, it varied within several kilotons. The Norwegian Sea occupies an intermediate position in this regard.

The increase of pCO_2 in surface waters within *E. huxlyei* blooms in the Barents Sea was most significant among the seas targeted in this study. In some years (2003, 2011) the resultant, $[(pCO_2)_b + \Delta pCO_2]$, partial CO_2 pressure was as high as ~350 μatm and practically never dropped below 250 μatm. The level of pCO2 in surface waters during the *E. huxleyi* bloom in the Norwegian Sea was the second highest after the Barents Sea, but most often it remained about 250 μatm. The Greenland Sea is the least active in terms of both production of extensive *E. huxleyi* blooms (Fig. 1) and enrichment of surface waters with dissolved CO_2 (Fig. 2).

The influence of *E. huxleyi* blooms on the hydrochemistry was nevertheless obviously significant in terms of enriching the marine surface water with both suspended carbon and dissolved carbon dioxide. So that, this phenomenon has a potential to both decrease the role of the World Oceans as sinkers of atmospheric CO_2, and affect the carbonate counter pump.

Acknowledgments

We express our thanks to Dr.D. Kondrik for his valuable help with data processing and discussions.

Благодарности

Выражаем благодарность к.г.н. Кондрику Дмитрию за его ценную помощь в работе с данными и обсуждения.

Funding

The present study was conducted and financially supported under St. Petersburg University Project No. 93016972.

Финансирование

Работа выполнена при финансовой поддержке Санкт-Петербургского государственного университета проект № 93016972.

References

1. IPCC, 2021: Climate Change 2021: The Physical Science Basis. Contribution of Working Group I to the Sixth Assessment Report of the Intergovernmental Panel on Climate Change [Masson-Delmotte, V., P. Zhai, A. Pirani, S.L. Connors, C. Péan, S. Berger, N. Caud, Y. Chen, L. Goldfarb, M.I. Gomis, M. Huang, K. Leitzell, E. Lonnoy, J.B.R. Matthews, T.K. Maycock, T. Waterfield, O. Yelekçi, R. Yu, and B. Zhou (eds.)]. Cambridge University Press, Cambridge, United Kingdom and New York, NY, USA, 2391 p. doi:10.1017/9781009157896.
2. *Burger F.*, *John J.G.*, *Frölicher T.L.* Increase in ocean acidity variability and extremes under increasing atmospheric CO_2. *Biogeosciences*. 2020, 17, 18, 4633–4662. doi:10.5194/bg-17-4633-2020
3. *Hauri C.*, *Pages R.*, *McDonnel A.M. P.* et al. Modulation of ocean acidification by decadal climate variability in the Gulf of Alaska. *Communications Earth & Environment*. 2021, 2, 191. doi:10.1038/s43247-021-00254-z
4. *Gattuso J.-P.*, *Brewer P.*, *Hoegh-Guldberg O.* Ocean acidification. Climate Change 2014: Impacts, Adaptation, and Vulnerability. Part A. Global and Sectoral Aspects / Contribution of Working Group II to the Fifth Assessment Report of the Intergovernmental Panel on Climate Change. (C.B. Field, V.R. Barros, and D.J. Dokken Eds). *Cambridge University Press*, *Cambridge*, *United Kingdom and New York*, *NY*, *USA*, 2014, P. 129–131.
5. *Thierstein H.R.*, *Young J.R.* Coccolithophores: From molecular processes to global impact. *Berlin*, *Springer*, 2004. 565 p. doi:10.1007/978-3-662-06278-4
6. *Pozdnyakov D.*, *Gnatiuk N.*, *Davy R.*, *Bobylev L.* The phenomenon of *Emiliania huxleyi* in aspects of global climate and The ecology of the World Ocean. *Geography*, *Environment*, *Sustainability*. 2021, 14, 2, 50–62. doi:10.24057/2071-9388-2020-214
7. *Kondrik D.V.*, *Pozdnyakov D.V.*, *Pettersson L.H.* Particulate inorganic carbon production within *E. huxleyi* blooms in subpolar and polar seas: a satellite time series study (1998–2013). *International Journal of Remote Sensing*. 2017, 38, 22, 6179–6205. doi:10.1080/01431161.2017.1350304
8. *Holligan P.M.*, et al. A biogeochemical study of the coccolithophore, *Emiliania huxleyi*, in the North Atlantic. *Global Biogeochemical Cycles*. 1993, 7, 4, 879–900. doi:10.1029/93GB01731
9. *Groom S.B.*, *Holligan P.M.* Remote sensing of coccolithophore blooms. *Advances in Space Research*. 1987, 7, 2, 73–78. doi:10.1016/0273-1177(87)90166-9
10. *Balch W.M.*, *Kilpatrick K.A.*, *Holligan P.M.*, *Harbour D.*, *Fernandez E.* The 1991 coccolithophore bloom in the central North Atlantic. 2. Relating optics to coccolith concentration. *Limnology and Oceanography*. 1996, 41, 8, 1684–1696. doi:10.4319/lo.1996.41.8.1684
11. *Brown C.W.*, *Yoder J.A.* Coccolithophoridblooms in the global ocean. *Journal of Geophysical Research*. 1994, 99, C4, 7467–7482. doi:10.1029/93JC02156
12. *Ackleson S.G.*, *Balch W.M.*, *Holligan P.M.* Response of water-leaving radiance to particulate calcite and chlorophyll *a* concentrations: A model for Gulf of Maine coccolithophore blooms. *Journal of Geophysical Research*: *Oceans*. Special Section. 1994, 99, C4, 7483–7499. doi:10.1029/93JC02150
13. *Smyth T.J.*, *Tyrrell T.*, *Tarrant B.* Time series of coccolithophore activity in the Barents Sea, from twenty years of satelliteimagery. *Geophysical Research Letters*. 2004, 31, 11. doi:10.1029/2004GL019735
14. *Cokacar T.*, *Oguz T.*, *Kubilay N.* Satellite-detected early summer coccolithophore blooms and their interannual variability in the Black Sea. *Deep Sea Research Part I*: *Oceanographic Research Papers*. 2004, 51, 8, 1017–1031. doi:10.1016/j.dsr.2004.03.007
15. *Burenkov V.I.*, *Kopelevich O.V.*, *Rat'kova T.N.*, *Sheberstov S.V.* Satellite observations of the coccolithophorid bloom in the Barents Sea. *Oceanology*. 2011, 51, 766–774. doi:10.1134/ S0001437011050043
16. *Iglesias-Rodriguez M.D.*, *Brown C.W.*, *Doney S.C.*, *Kleypas J.*, *Kolber D.*, *Kolber Z.*, *Hayes P.K.*, *Falkowski P.G.* Representing key phytoplankton functional groups in ocean carbon cycle models: Coccolithophorids. *Global Biogeochemical Cycles*. 2002, 16, 4, 47–1–47–20. doi:10.1029/2001GB001454
17. *Moore T.*, *Dowel M.D.*, *Franz B.A.* Detection of coccolithophore blooms in ocean color imagery: A generalized approach for use with multiple sensors. *Remote Sensing of Environment*. 2012, 117, 249–263. doi:10.1016/j.rse.2011.10.001

18. *Sadeghi A.*, *Dinter T.*, *Vountas M.*, *Taylor B.*, *Altenburg-Soppa M.*, *Bracher A.* Remote sensing of coccolithophore blooms in selected oceanic regions using the PhytoDOAS method applied to hyper-spectral satellite data. *Biogeosciences*. 2012, 9, 6, 2127–2143. doi:10.5194/bg-9-2127-2012
19. *Balch W.M.*, *Drapeau D.T.*, *Bowler B.C.*, *Lyczkowski E.R.*, *Lubelczyk L.C.*, *Painter S.C.*, *Poulton A.J.* Surface biological, chemical, and optical properties of the Patagonian Shelf coccolithophore bloom, the brightest waters of the Great Calcite Belt. *Limnology and Oceanography*. 2014, 59, 5, 1715–1732. doi:10.4319/lo.2014.59.5.1715
20. *Iida T.*, *Saitoh S.I.*, *Miyamura T.*, *Toratani M.*, *Fukushima H.*, *Shiga N.* Temporal and spatial variability of coccolithophore blooms in the eastern Bering Sea, 1998–2001. *Progress in Oceanography*. 2002, 55, 1–2, 165–175. doi:10.1016/S0079-6611(02)00076-9
21. *Merico A.*, *Tyrrell T.*, *Brown C.W.*, *Groom S.B.*, *Miller P.I.* Analysis of satellite imagery for *Emiliania huxleyi* blooms in the Bering Sea before 1997. *Geophysical Research Letters*. 2003, 30, 6, 1337. doi:10.1029/2002GL016648
22. *Petrenko D.A.*, *Zabolotskikh E.V.*, *Pozdnyakov D.V.*, *Counillon F.*, *Karlin L.N.* Interannual variations and trend of the production of inorganic carbon by coccolithophores in the arctic in 2002–2010 based on satellite data. *Izvestiya*, *Atmospheric and Oceanic Physics*. 2013, 49, 871–878. doi:10.1134/S0001433813090119
23. *Kopelevich O.*, *Burenkov V.*, *Sheberstov S.*, *Vazyulya S.*, *Kravchishina M.*, *Pautova L.*, *Silkin V.*, *Artemiev V.*, *Grigoriev A.* Satellite monitoring of coccolithophore blooms in the Black Sea from ocean color data. *Remote Sensing of Environment*. 2014, 146, 113–123. doi:10.1016/j.rse.2013.09.009
24. *Kondrik D.V.*, *Pozdnyakov D.V.*, *Johannessen O.M.* Satellite evidence that *E. huxleyi* phytoplankton blooms weaken marine carbon sinks. *Geophysical Research Letters*. 2018, 45, 2, 846–854. doi:10.1002/2017GL076240
25. *Morozov E.A.*, *Kondrik D.V.*, *Chepikova S.S.*, *Pozdnyakov D.V.* Atmospheric columnar CO_2 enhancement over *E. huxleyi* blooms: case studies in the North Atlantic and Arctic waters. *Transactions of the Karelian Research Centre, RAS. Limnology and Oceanography*. 2019, 3, 28–33. doi: 10.17076/lim989
26. *Pozdnyakov D.V.*, *Pettersson L.H.*, *Korosov A.A.* Exploring the marine ecology from space. Experience from Russian-Norwegian Cooperation. Series: Springer Remote Sensing/Photogrammetry. *Heidelberg*, *New York*, *Dordrecht*, *London*, *Springer*, 2017. 215 p.
27. The Copernicus Marine Environment Monitoring Service (*CMEMS*). 2015: Globcolour project, L3 Ocean Colour products. URL: http://globcolour.info (date of access: 10.10.2021).
28. *Garnesson P.*, *Mangin A.*, *d'Andon O.F.*, *Demaria J.*, *Bretagnon M.* The CMEMS GlobColour *chlorophyll-a* product based on satellite observation: multi-sensor merging and flagging strategies. *Ocean Science*. 2019, 15, 819–830, doi:10.5194/os-15-819-2019
29. *Snyder J.P.* Map projections: A working manual. Professional paper 1395. *Washington*, *DC*, *US Geological Survey*, 1987. 305 p.
30. NOAA National Geophysical Data Center. 2018: AVHRR Pathfinder version 5.3 level 3 collated (L3C) global 4km sea surface temperature for 1981-Present. NOAA National Centers for Environmental Information. Dataset. URL: https://data.nodc.noaa.gov/cgi-bin/iso?id=gov.noaa.nodc: AVHRR_Pathfinder-NCEI–L3C-v5.3 (date of access: 10.05.2022). doi:10.7289/v52j68xx
31. *Casey K.S.*, *Brandon T.B.*, *Cornillon P.*, *Evans R.* The past, present and future of the AVHRR pathfinder SST program. *Oceanography from Space*: *Revisited* / eds. V. Barale, J.F.R. Gower, and L. Alberotanza, *Springer*, 2010. doi:10.1007/978-90-481-8681-5_16
32. *Korak S.*, *Zhao X.Z.*, *Zhang H.*, *Casey S.*, *Zhang D.*, *Baker-Yeboah S.*, *Kilpatrick K.A.*, *Evans R.H.*, *Ryan T.*, *Relph J.M.* AVHRR Pathfinder version 5.3 level 3 collated (L3C) global 4km sea surface temperature for 1981-Present. *NOAA National Centers for Environmental Information*. 2018, *Dataset*. doi:10.7289/v52j68xx
33. NOAA National Geophysical Data Center. 2018: The World Ocean Atlas. NOAA National Centers for Environmental Information. URL: https://www.ncei.noaa.gov/products/world-ocean-atlas (date of access: 10.05.2022).
34. *Jerome J.H.*, *Bukata R.P.*, *Miller J.R.* Remote sensing reflectance and its relationship to optical properties of natural water. *International Journal of Remote Sensing*. 1996, 17, 16, 3135–3155. doi:10.1080/01431169608949135
35. *Sokoletsky L.G.*, *Lunetta R.S.*, *Wetz M.S.*, *Paerl H.W.* Assessment of the water quality components in turbid estuarine waters based on radiative transfer approximations. *Israel Journal of Plant Sciences*. 2012, 60, 209–229. doi:10.1560/IJPS.60.1–2.209
36. *Press W.*, *Teukolsky S.*, *Vettering W.*, *Flannery B.* Numerical recipes in C: The art of scientific computing. 2nd ed. *New York*, *Cambridge University Press*, 1992. 1262 p.
37. *Balch W.M.*, *Gordon H.*, *Bowler B.C.*, *Drapeau D.T.*, *Booth E.S.* Calcium carbonate measurements in the surface global ocean based on Moderate-Resolution Imaging Spectrometer Data. *Journal of Geophysical Research*. 2005, 110, C7, C07001. doi:10.1029/ 2004JC002560
38. *Montegut C.*, *Madec G.*, *Fisher A.*, *Lazar A.*, *Iudicone D.* Mixed layer depth over the global ocean: An examination of profile data and a profile-based climatology. *Journal of Geophysical Research*. 2004, 109, C12, C12003. doi:10.1029/2004JC002378

39. *Honjo S.* Coccoliths: Production, transportation and sedimentation. *Marine Micropaleontology*. 1976, 1, 65–79. doi:10.1016/0377–8398(76)90005–0

40. *Pozdnyakov D.V.*, *Chepikova S.*, *Kondrik D.V.* A possible teleconnection mechanism of initiation of *Emiliania huxleyi* outbursts in the Bering Sea in 1998–2001 and 2018–2019. *Proceedings Volume 11534*, *Earth Resources and Environmental Remote Sensing/GIS Applications XI*; 1153412, 2020. doi:10.1117/12.2573272

41. *Pozdnyakov D.*, *Kondrik D.*, *Kazakov E.*, *Chepikova S.* Environmental conditions favoring coccolithophore blooms in subarctic and arctic seas: a 20-year satellite and multi-dimensional statistical study. *SPIE Proceedings*, *11150*: *SPIE*: *Remote Sensing of the Ocean*. *9–12 September Strasbourg, France*, 2019. doi:10.1117/12.2547868

Литература

1. IPCC, 2021: Climate Change 2021: The Physical Science Basis. Contribution of Working Group I to the Sixth Assessment Report of the Intergovernmental Panel on Climate Change [Masson-Delmotte, V., P. Zhai, A. Pirani, S.L. Connors, C. Péan, S. Berger, N. Caud, Y. Chen, L. Goldfarb, M.I. Gomis, M. Huang, K. Leitzell, E. Lonnoy, J.B.R. Matthews, T.K. Maycock, T. Waterfield, O. Yelekçi, R. Yu, and B. Zhou (eds.)]. Cambridge University Press, Cambridge, United Kingdom and New York, NY, USA, 2391 p. doi:10.1017/9781009157896

2. *Burger F.*, *John J.G.*, *Frölicher T.L.* Increase in ocean acidity variability and extremes under increasing atmospheric CO_2 // Biogeosciences. 2020. Vol. 17, Iss. 18. P. 4633–4662. doi:10.5194/bg-17–4633–2020

3. *Hauri C.*, *Pages R.*, *McDonnel A.M. P.* et al. Modulation of ocean acidification by decadal climate variability in the Gulf of Alaska // Communications Earth & Environment. 2021. Vol. 2. Art. 191. doi:10.1038/s43247–021–00254-z

4. *Gattuso J.-P.*, *Brewer P.*, *Hoegh-Guldberg O.* Ocean acidification // Climate Change 2014: Impacts, Adaptation, and Vulnerability. Part A. Global and Sectoral Aspects / Contribution of Working Group II to the Fifth Assessment Report of the Intergovernmental Panel on Climate Change. (C.B. Field, V.R. Barros, and D.J. Dokken Eds). Cambridge University Press, Cambridge, United Kingdom and New York, NY, USA, 2014, P. 129–131.

5. *Thierstein H.R.*, *Young J.R.* Coccolithophores: From molecular processes to global impact. Berlin: Springer, 2004. 565 p. doi:10.1007/978-3-662-06278-4

6. *Pozdnyakov D.*, *Gnatiuk N.*, *Davy R.*, *Bobylev L.* The phenomenon of *Emiliania huxleyi* in aspects of global climate and the ecology of the World Ocean // Geography, Environment, Sustainability. 2021. Vol. 14, N 2. P. 50–62. doi:10.24057/2071-9388-2020-214

7. *Kondrik D.V.*, *Pozdnyakov D.V.*, *Pettersson L.H.* Particulate inorganic carbon production within *E. huxleyi* blooms in subpolar and polar seas: a satellite time series study (1998–2013) // International Journal of Remote Sensing. 2017. Vol. 38, Iss. 22, P. 6179–6205. doi:10.1080/01431161.2017.1350304

8. *Holligan P.M.*, et al. A biogeochemical study of the coccolithophore, *Emiliania huxleyi*, in the North Atlantic // Global Biogeochemical Cycles. 1993. Vol. 7, Iss. 4. P. 879–900. doi:10.1029/93GB01731

9. *Groom S.B.*, *Holligan P.M.* Remote sensing of coccolithophore blooms // Advances in Space Research. 1987. Vol. 7, Iss. 2. P. 73–78. doi:10.1016/0273–1177(87)90166–9

10. *Balch W.M.*, *Kilpatrick K.A.*, *Holligan P.M.*, *Harbour D.*, *Fernandez E.* The 1991 coccolithophore bloom in the central North Atlantic. 2. Relating optics to coccolith concentration // Limnology and Oceanography. 1996. Vol. 41, Iss. 8. P. 1684–1696. doi:10.4319/lo.1996.41.8.1684

11. *Brown C.W.*, *Yoder J.A.* Coccolithophoridblooms in the global ocean // Journal of Geophysical Research. 1994. Vol. 99, Iss. C4. P. 7467–7482. doi:10.1029/93JC02156

12. *Ackleson S.G.*, *Balch W.M.*, *Holligan P.M.* Response of water-leaving radiance to particulate calcite and chlorophyll *a* concentrations: A model for Gulf of Maine coccolithophore blooms // Journal of Geophysical Research: Oceans. Special Section. 1994. Vol. 99, Iss. C4. P. 7483–7499. doi:10.1029/93JC02150

13. *Smyth T.J.*, *Tyrrell T.*, *Tarrant B.* Time series of coccolithophore activity in the Barents Sea, from twenty years of satelliteimagery // Geophysical Research Letters. 2004. Vol. 31, Iss. 11. doi:10.1029/2004GL019735

14. *Cokacar T.*, *Oguz T.*, *Kubilay N.* Satellite-detected early summer coccolithophore blooms and their interannual variability in the Black Sea // Deep Sea Research Part I: Oceanographic Research Papers. 2004. Vol. 51, Iss. 8. P. 1017–1031. doi:10.1016/j.dsr.2004.03.007

15. *Буренков В.И.*, *Копелевич О.В.*, *Ратькова Т.Н.*, *Шеберстов С.В.* Спутниковые наблюдения цветения кокколитофорид в Баренцевом море // Океанология. 2011. Т. 51. № 5. С. 818–826.

16. *Iglesias-Rodriguez M.D.*, *Brown C.W.*, *Doney S.C.*, *Kleypas J.*, *Kolber D.*, *Kolber Z.*, *Hayes P.K.*, *Falkowski P.G.* Representing key phytoplankton functional groups in ocean carbon cycle models: Coccolithophorids // Global Biogeochemical Cycles. 2002. Vol. 16, Iss. 4. P. 47–1–47–20. doi:10.1029/2001GB001454

17. *Moore T.*, *Dowel M.D.*, *Franz B.A.* Detection of coccolithophore blooms in ocean color imagery: A generalized approach for use with multiple sensors // Remote Sensing of Environment. 2012. Vol. 117. P. 249–263. doi:10.1016/j.rse.2011.10.001

18. *Sadeghi A.*, *Dinter T.*, *Vountas M.*, *Taylor B.*, *Altenburg-Soppa M.*, *Bracher A.* Remote sensing of coccolithophore blooms in selected oceanic regions using the PhytoDOAS method applied to hyper-spectral satellite data // Biogeosciences. 2012. Vol. 9, Iss. 6. P. 2127–2143. doi:10.5194/bg-9-2127-2012
19. *Balch W.M.*, *Drapeau D.T.*, *Bowler B.C.*, *Lyczkowski E.R.*, *Lubelczyk L.C.*, *Painter S.C.*, *Poulton A.J.* Surface biological, chemical, and optical properties of the Patagonian Shelf coccolithophore bloom, the brightest waters of the Great Calcite Belt // Limnology and Oceanography. 2014. Vol. 59, Iss. 5. P. 1715–1732. doi:10.4319/lo.2014.59.5.1715
20. *Iida T.*, *Saitoh S.I.*, *Miyamura T.*, *Toratani M.*, *Fukushima H.*, *Shiga N.* Temporal and spatial variability of coccolithophore blooms in the eastern Bering Sea, 1998–2001 // Progress in Oceanography. 2002. Vol. 55, Iss. 1–2. P. 165–175. doi:10.1016/S0079–6611(02)00076–9
21. *Merico A.*, *Tyrrell T.*, *Brown C.W.*, *Groom S.B.*, *Miller P.I.* Analysis of satellite imagery for *Emiliania huxleyi* blooms in the Bering Sea before 1997 // Geophysical Research Letters. 2003. Vol. 30, Iss. 6. 1337. doi:10.1029/2002GL016648
22. *Петренко Д.А.*, *Заболотских Е.В.*, *Поздняков Д.В.*, *Кунийон Ф.*, *Карлин Л.Н.* Межгодовые вариации и тренд продукции неорганического углерода кокколитофорного происхождения в Арктике за период 2002–2010 гг. по спутниковым данным // Исследование Земли из космоса. 2013. № 2. С. 19–27. doi:10.7868/S0205961413020085
23. *Kopelevich O.*, *Burenkov V.*, *Sheberstov S.*, *Vazyulya S.*, *Kravchishina M.*, *Pautova L.*, *Silkin V.*, *Artemiev V.*, *Grigoriev A.* Satellite monitoring of coccolithophore blooms in the Black Sea from ocean color data // Remote Sensing of Environment. 2014. Vol. 146. P. 113–123. doi:10.1016/j.rse.2013.09.009
24. *Kondrik D.V.*, *Pozdnyakov D.V.*, *Johannessen O.M.* Satellite evidence that *E. huxleyi* phytoplankton blooms weaken marine carbon sinks // Geophysical Research Letters. 2018. Vol. 45, Iss. 2. P. 846–854. doi:10.1002/2017GL076240
25. *Морозов Е.А.*, *Кондрик Д.В.*, *Чепикова С.С.*, *Поздняков Д.В.* Увеличение концентрации CO_2 в атмосферном столбе над областью цветения *E. huxleyi*: конкретные случаи в водах Северной Атлантики и Арктики // Труды Карельского научного центра РАН. Серия Лимнология и океанология. 2019. № 3. С. 28–33. doi:10.17076/lim989
26. *Pozdnyakov D.V.*, *Pettersson L.H.*, *Korosov A.A.* Exploring the marine ecology from space. Experience from Russian-Norwegian Cooperation. Series: Springer Remote Sensing/Photogrammetry. Heidelberg, New York, Dordrecht, London: Springer, 2017. 215 p.
27. The Copernicus Marine Environment Monitoring Service (*CMEMS*). 2015: Globcolour project, L3 Ocean Colour products. URL: http://globcolour.info (дата обращения: 10.10.2021).
28. *Garnesson P.*, *Mangin A.*, *d'Andon O.F.*, *Demaria J.*, *Bretagnon M.* The CMEMS GlobColour *chlorophyll-a* product based on satellite observation: multi-sensor merging and flagging strategies // Ocean Science. 2019. Vol. 15. P. 819–830. doi:10.5194/os-15–819–2019
29. *Snyder J.P.* Map projections: A working manual. Professional paper 1395. Washington, DC, US Geological Survey, 1987. 305 p.
30. NOAA National Geophysical Data Center. 2018: AVHRR Pathfinder version 5.3 level 3 collated (L3C) global 4km sea surface temperature for 1981-Present. NOAA National Centers for Environmental Information. Dataset. URL: https://data.nodc.noaa.gov/cgi-bin/iso?id=gov.noaa.nodc: AVHRR_Pathfinder-NCEI–L3C-v5.3 (дата обращения: 10.05.2022). doi:10.7289/v52j68xx
31. *Casey K.S.*, *Brandon T.B.*, *Cornillon P.*, *Evans R.* The past, present and future of the AVHRR pathfinder SST program // Oceanography from Space: Revisited / eds. V. Barale, J.F.R. Gower, and L. Alberotanza, Springer. 2010. doi:10.1007/978–90–481–8681–5_16
32. *Korak S.*, *Zhao X.Z.*, *Zhang H.*, *Casey S.*, *Zhang D.*, *Baker-Yeboah S.*, *Kilpatrick K.A.*, *Evans R.H.*, *Ryan T.*, *Relph J.M.* AVHRR Pathfinder version 5.3 level 3 collated (L3C) global 4km sea surface temperature for 1981-Present // NOAA National Centers for Environmental Information. 2018, Dataset. doi:10.7289/v52j68xx
33. NOAA National Geophysical Data Center. 2018: The World Ocean Atlas. NOAA National Centers for Environmental Information. URL: https://www.ncei.noaa.gov/products/world-ocean-atlas (дата обращения: 10.05.2022).
34. *Jerome J.H.*, *Bukata R.P.*, *Miller J.R.* Remote sensing reflectance and its relationship to optical properties of natural water // International Journal of Remote Sensing. 1996. Vol. 17, Iss. 16. P. 3135–3155. doi:10.1080/01431169608949135
35. *Sokoletsky L.G.*, *Lunetta R.S.*, *Wetz M.S.*, *Paerl H.W.* Assessment of the water quality components in turbid estuarine waters based on radiative transfer approximations // Israel Journal of Plant Sciences. 2012. Vol. 60. P. 209–229. doi:10.1560/IJPS.60.1–2.209
36. *Press W.*, *Teukolsky S.*, *Vettering W.*, *Flannery B.* Numerical recipes in C: The art of scientific computing. 2nd ed. New York: Cambridge University Press, 1992. 1262 p.
37. *Balch W.M.*, *Gordon H.*, *Bowler B.C.*, *Drapeau D.T.*, *Booth E.S.* Calcium carbonate measurements in the surface global ocean based on Moderate-Resolution Imaging Spectrometer Data // Journal of Geophysical Research. 2005. Vol. 110, Iss. C7. C07001. doi:10.1029/ 2004JC002560
38. *Montegut C.*, *Madec G.*, *Fisher A.*, *Lazar A.*, *Iudicone D.* Mixed layer depth over the global ocean: An examination of profile data and a profile-based climatology // Journal of Geophysical Research. 2004. Vol. 109, Iss. C12. C12003. doi:10.1029/2004JC002378

39. *Honjo S.* Coccoliths: Production, transportation and sedimentation // Marine Micropaleontology. 1976. Vol. 1. P. 65–79. doi:10.1016/0377–8398(76)90005–0

40. *Pozdnyakov D.V.*, *Chepikova S.*, *Kondrik D.V.* A possible teleconnection mechanism of initiation of *Emiliania huxleyi* outbursts in the Bering Sea in 1998–2001 and 2018–2019 // Proceedings Volume 11534, Earth Resources and Environmental Remote Sensing/GIS Applications XI; 1153412. 2020. doi:10.1117/12.2573272

41. *Pozdnyakov D.*, *Kondrik D.*, *Kazakov E.*, *Chepikova S.* Environmental conditions favoring coccolithophore blooms in subarctic and arctic seas: a 20-year satellite and multi-dimensional statistical study // SPIE Proceedings,11150: SPIE: Remote Sensing of the Ocean. 9–12 September Strasbourg, France, 2019. doi:10.1117/12.2547868

About the authors

FROLOVA Anastasiia Valeryevna, РИНЦ Author ID: 1124673, ORCID ID: 0000-0002-8064-7116, Scopus Author ID: 57210446164, WoS ResearcherID: ACE-4108–2022, st050263@student.spbu.ru

POZDNYAKOV Dmitry Victorovich, РИНЦ Author ID: 179336, ORCID ID: 0000-0003-0889-7855, Scopus Author ID: 56370460300, dmitry.pozdnyakov@niersc.spb.ru

MOROZOV Evgeny Aleksandrovich, РИНЦ Author ID: 1115348, Scopus Author ID: 57193680029, WoS ResearcherID: F-9030–2017